

# Energetics of rotary-wing exploration of Titan

Jack W. Langelaan, Sven Schmitz, Jose Palacios  
Aerospace Engineering  
Penn State University  
University Park, PA  
jlangelaan@psu.edu  
tel: 1-814-863-6817

Ralph D. Lorenz  
Johns Hopkins University Applied Physics Lab  
Laurel, MD  
Ralph.Lorenz@jhuapl.edu  
tel: 1-443-778-2903

**Abstract**—Rotary-wing vehicles have the potential to enable exploration of Titan at scales ranging from hundreds of kilometers to millimeters. This paper examines the flight power demands of multi-rotor vehicles (e.g. quadcopters or co-axial helicopters), considering both hover and forward flight. Specifically, this paper examines power demands of a small (1 kg) co-axial helicopter as well as a larger (350 kg) multi-rotor vehicle. In both cases the power requirements are well within the capabilities of current batteries and electric motors: the 350 kg vehicle requires 1.87 kW aerodynamic power for hover and 1.32 kW aerodynamic power for cruise at an airspeed of 9.5 m/s; the 1 kg vehicle requires 3.63 W aerodynamic power for hover and 3.17 W aerodynamic power to cruise at 4 m/s. Energy requirements of the 1 kg vehicle are driven mainly by thermal management and power required by avionics: this has a significant influence on range, endurance, and optimal flight speeds. The flight performance characteristics of both vehicles are capable of fulfilling meaningful scientific goals.

## TABLE OF CONTENTS

1. INTRODUCTION.....	1
2. MISSION AND VEHICLE CONSTRAINTS.....	2
3. VEHICLE AND ROTOR AND CONCEPTUAL DESIGN..	2
4. ENERGETICS OF ROTARY-WING FLIGHT .....	5
5. PERFORMANCE AND SENSITIVITY .....	6
6. CONCLUSION .....	9
REFERENCES .....	10
BIOGRAPHY .....	11

## 1. INTRODUCTION

As a unique icy moon with a thick atmosphere and an organic-rich surface, Titan is an appealing target for scientific exploration. The arrival of Cassini in 2004 and release of the Huygens probe in January 2005 gave planetary scientists the first *in situ* measurements of conditions on Titan. After a 2.5-hour parachute descent, the Huygens probe landed on a (methane-damp) alluvial plane littered with icy cobbles, and operated for several hours before its battery expired. Since then, Cassini's radar and other instruments have shown Titan's surface to be remarkably varied, with mountains, dunefields, plains, lakes and seas. This diversity motivates consideration of mobility in the near-surface environment, and previous 'Flagship' mission studies of Titan, including that advocated in the 2012 Planetary Science Decadal Survey, have included elements with such capability (specifically, hot air balloons).

Many researchers have pointed out the potential for flight-based exploration of Titan [1], [2], [3], [4]. This potential for flight is entirely based on the high density of Titan's

atmosphere, which reduces the wing area (or disc area, in the case of rotary-wing vehicles) required to generate a given amount of lift force, and on the low gravity of Titan, which reduces the required magnitude of lift force. Since the power required for steady level flight scales as  $(mg)^{1.5}$ , Titan's lower gravitational acceleration reduces the power required for flight by a factor of 19 when compared with an Earth-based fixed-wing aircraft.

Additionally, Titan's higher atmospheric density means that for a given wing loading, less power is required to sustain flight. Alternatively, wing loading can be increased (i.e. wing area reduced), resulting in easier packaging in the launch vehicle. Combining Titan's low gravity and high density implies that an aircraft with a given wing area and flight velocity can lift 28 times more mass on Titan than on Earth [5]. Titan's low kinematic viscosity means that inertial forces will dominate aerodynamics at the scales of vehicles that have been considered.

A concept for a fixed-wing Titan explorer called AVIATR is described in detail in Barnes et al. [5]. Its total mass is 115.75 kg and it requires 115 W in steady level flight. This mission was predicated on the availability of Advanced Stirling Radioisotope Generators (ASRG) for flight power.

Lighter-than-air (LTA) explorers such as balloons and blimps are described in Reh et al. [6] and Lorenz [7]. Balloon explorers have limited control over flight path: altitude can be changed, allowing winds at different altitudes to be exploited for some flight path control, but access to surface materials (required for key 'Ocean Worlds' scientific goals) poses significant challenges. Levine describes a blimp with 89 m<sup>3</sup> total displacement, 378 kg total mass, and 4 m/s maximum air speed [8]. Power is obtained from four SRGs. Hall et al. describe an aerobot with 60 m<sup>3</sup> total displacement and 232 kg total mass [9].

The properties that make Titan an attractive place for fixed-wing aircraft and LTA flight vehicles also make it favorable for rotary-wing aircraft such as helicopters, tiltrotors, and multi-copters. Indeed, rotary-wing aircraft provide a key advantage over both fixed-wing and LTA aircraft: the ability to perform repeated precision soft landings.

An outstanding post-Cassini science knowledge gap is the composition of the various surface units. While some remote composition measurements might be made from an aerial platform, these are inevitably limited in capability, and safe maneuvering of a balloon or airship near the surface is challenging. Various concepts devised to acquire surface samples from a balloon (e.g. a tethered 'harpoon' [10]) have been inventive, but remain unconvincing without further study. Similarly, conventional landers are effective for surface access, but are limited to a single location on what Cassini has shown to be a very complex and diverse surface. Wheeled

rovers have proven successful on Mars, but the possibility of wheeled mobility on Titan is still unknown. On the other hand, rotorcraft are tailor-made for surface access, by permitting vertical soft-landing at designated locations and once the rotors are powered down, the vehicle weight facilitates drilling or other sampling operations. While the studies of rotary-wing Titan exploration systems have lagged that of both fixed-wing and LTA systems, there have been some brief descriptions of potential concepts (e.g. [1] advocated a Titan helicopter on scientific grounds). Prakash et al. describe a 318 kg vehicle with conventional helicopter configuration (3.2m diameter main rotor, 0.6m diameter tail rotor) [11]. A much smaller vehicle called Bumblebee (essentially a 1 kg mass vertical take-off airplane, rather than a rotorcraft *per se*) is described in Lorenz [3].

## 2. MISSION AND VEHICLE CONSTRAINTS

Clearly, any Titan flight vehicle must fit inside the aeroshell required for entry into Titan's atmosphere. For fixed wing aircraft, folding wings have generally been assumed; for some rotary wing aircraft, it is possible to fit the vehicle in the aeroshell without folding rotors (Figure 1a).

Power required for flight scales inversely with the square root of disc area. Interestingly (and perhaps counter-intuitively), the net disc area of some multi rotors that fit into an aeroshell of given diameter is greater than the disc area of a conventional helicopter that fits into the same aeroshell. To establish an upper bound on available disc area, consider a multi rotor with  $N_R$  2-bladed rotors that fits into an aeroshell with radius  $R$ . Further, assume that each individual rotor disc cannot overlap. Note that each rotor forms a chord inside the aeroshell (see Figure 1). The dash-dot line shows the aeroshell, the grey line shows the radial locations of the rotor hubs, and the rotors are shown as black lines with a grey region defining the rotor disc.

Referring to Figure 1a, the radial locations of the rotor hubs  $c$  and the rotor radius  $r$  are functions of the number of rotors  $N_R$ , and the aeroshell radius  $R$ :

$$\frac{r}{c} = \sin \frac{\pi}{N} \quad (1)$$

$$r^2 + c^2 = R^2 \quad (2)$$

Hence

$$r^2 = R^2 \frac{\sin^2 \frac{\pi}{N}}{1 + \sin^2 \frac{\pi}{N}} \quad (3)$$

and the net disc area for  $N$  rotors is

$$A_{net} = N\pi r^2 = N\pi R^2 \frac{\sin^2 \frac{\pi}{N}}{1 + \sin^2 \frac{\pi}{N}} \quad (4)$$

The upper plot of Figure 1b shows the variation in net disc area with number of rotors for an aeroshell with radius  $R = 1.5$  m assuming "packaging" as shown in Figure 1a. It also shows the "open area" (the area of a circle inscribed within the rotors that will not be in the downwash). If the vehicle's fuselage can fit into this open area, rotor efficiency will not be adversely affected by the fuselage.

The disc area fraction is net disc area divided by aeroshell

projected area:

$$f_{disc} = \frac{A_{net}}{\pi R^2} = N \frac{\sin^2 \frac{\pi}{N}}{1 + \sin^2 \frac{\pi}{N}} \quad (5)$$

Four rotors provides a 33% increase in net disc area and provides a small open area for the center body; six rotors provides a 20% increase in net disc area and provides an open area equal to the disc area of one rotor; eight rotors provides a net disc area 2% greater than that provided by a single large rotor and provides an open area equal to 33% of the net aeroshell projected area. Above eight rotors, the net disc area drops below that provided by a single large rotor, and as  $N \rightarrow \infty$  the net disc area approaches zero. Hence if more than eight rotors are required (e.g. because the power or torque loading of a single rotor is still too high) then co-axial rotors should be considered.

The lower plot of Figure 1b shows that for this packaging, the greatest possible net disc area occurs with four rotors. Note, however, that other constraints may affect the optimal rotor configuration: the vehicle body must also fit into the aeroshell along with the rotors. Further, the large net disc area provided by four rotors may be somewhat offset if the vehicle body is placed above or below the rotor plane and interferes with rotor in-flow or out-flow.

In addition to increasing net disc area, increasing the number of rotors (up to a maximum of eight) provides the following benefits: (a) rigid, fixed-pitch rotors can be used when  $N \geq 4$ , simplifying hub design; (b) the power and torque of an individual motor is reduced; (c) control redundancy is increased, improving fault tolerance and providing a larger space for control allocation and trim condition optimization; (d) motor/rotor combinations are likely to have lower inertia, improving control response.

Note, however, that other effects can become important. Smaller rotors typically operate at lower Reynolds number, so viscous losses will become greater. The additional structure required to carry thrust loads (although each rotor's thrust load becomes smaller as the number of rotors increases) will add complication (and perhaps weight).

## 3. VEHICLE AND ROTOR AND CONCEPTUAL DESIGN

A reason for the comparative lack of Titan rotorcraft studies may be the perceived power requirements of rotary-wing versus fixed-wing aircraft. As mentioned earlier, both Titan's atmospheric properties and its low gravity mean that flight requires significantly less power than on Earth. Key parameters relevant to flight on both Titan and Earth are given in Table 1 and Figure 2.

A measure of power required by a rotary-wing vehicle is ideal hover power, which is derived using momentum theory [12]:

$$P_i = \sqrt{\frac{m^3 g^3}{2\rho A}} \quad (6)$$

where  $m$  is vehicle mass,  $g$  is acceleration due to gravity,  $\rho$  is atmospheric density and  $A$  is the rotor disc area.

Figure 3 shows ideal hover power as a function of vehicle mass and rotor disc area: a 115 kg rotorcraft (similar in

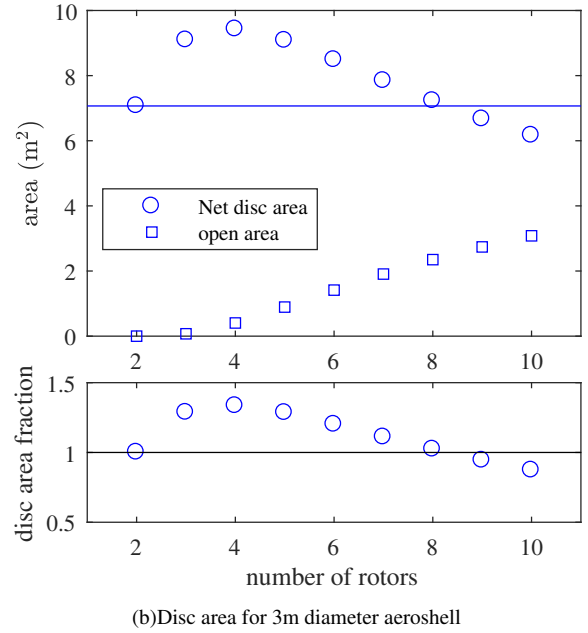
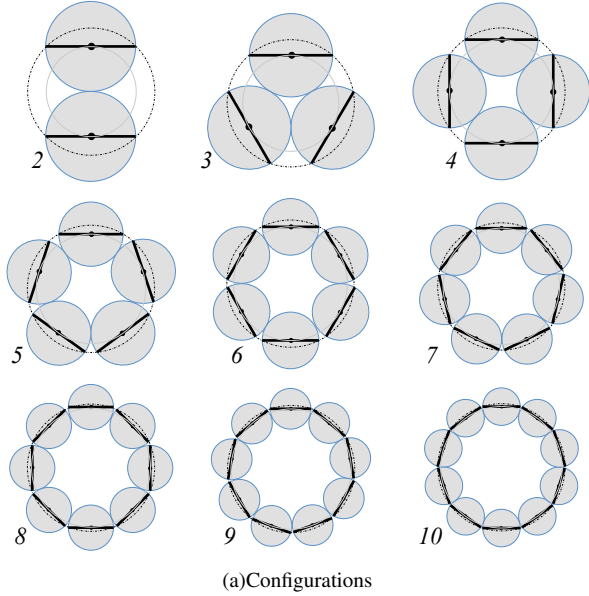


Figure 1. Schematics of multirotor configurations sized to fit inside an aeroshell.

Table 1. Comparison of surface-level parameters on Titan and Earth (ICAO Standard Atmosphere)

Parameter	Symbol	Titan	Earth	Titan/Earth
gravitational acceleration	$g$	$1.35 \text{ m s}^{-2}$	$9.81 \text{ m s}^{-2}$	0.14
atmospheric density	$\rho$	$5.428 \text{ kg m}^{-3}$	$1.225 \text{ kg m}^{-3}$	4.43
kinematic viscosity	$\nu$	$1.23 \times 10^{-6} \text{ m}^2 \text{ s}^{-1}$	$1.46 \times 10^{-5} \text{ m}^2 \text{ s}^{-1}$	0.084
sound speed	$a$	$195 \text{ m s}^{-1}$	$340 \text{ m s}^{-1}$	0.57

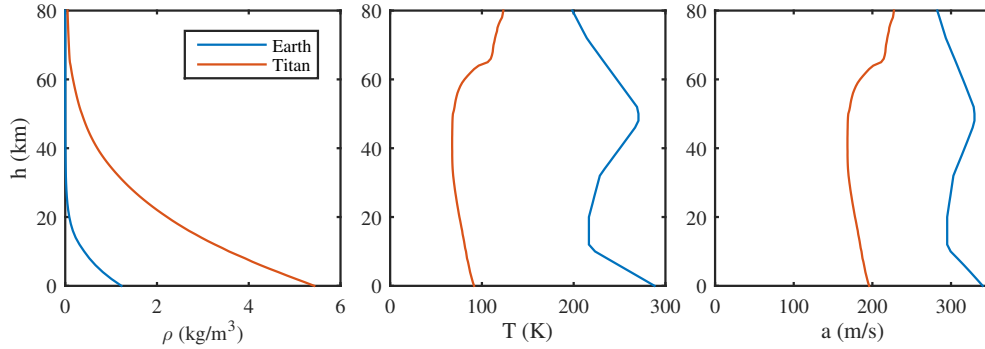


Figure 2. Comparison of atmospheric profiles of Titan and Earth.

weight to AVIATR) a single 3m diameter rotor (resulting in disc area  $7.07 \text{ m}^2$ ) has an ideal hover power of 221 W. This is above the capabilities of ASRG and MMRTG (Multi-Mission Radioisotope Thermoelectric Generator- a roughly 100W power source that is presently in operation on the Mars Science Laboratory Curiosity), but is well within the capabilities of electric motors and batteries. A quadrotor that fits into a 3m diameter aeroshell has maximum net disc area  $9.4 \text{ m}^2$ , reducing ideal hover power to 191 W. The hover power of even a large quad-rotor (500 kg) is 1736 W, well within the capabilities of currently-available motors and batteries. Actual hover power is typically 25-30% greater than ideal hover power, and depends on the specifics of rotor and vehicle design.

Thus rather than continuous flight, a more realistic rotorcraft mission on Titan may consist of a sequence of flights of a few tens of kilometers on battery power followed by landing and battery recharge from an MMRTG. This concept of brief hops between long recharge during the Titan night was proposed by Lorenz [1], [13].

#### Rotor design considerations

Preliminary rotor parameters can be determined from the constraints imposed by the vehicle and mission (e.g. mass, rotor diameter, number of rotors) and an initial value for the average blade section lift coefficient  $\bar{c}_l$ . This initial section lift coefficient will affect rotor tip speed and thus the operating Reynolds number, the power required to overcome profile

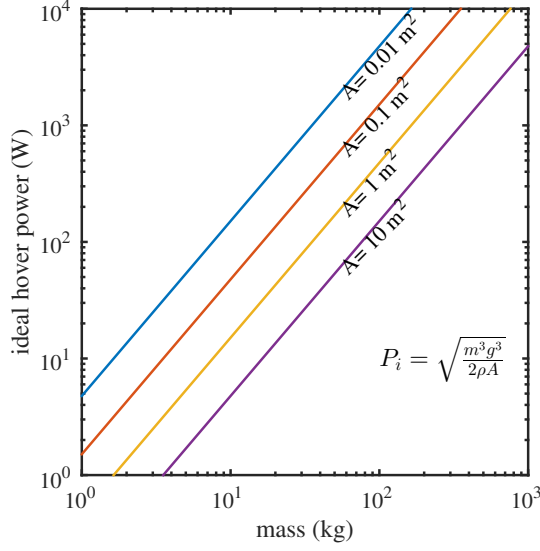


**Figure 3. Ideal hover power as a function of vehicle mass and rotor disc area.**

drag, and advance ratio in forward flight.

From [12], the mean blade section lift coefficient  $\bar{c}_l$  in hover is

$$\bar{c}_l = \frac{6C_T}{\sigma} \quad (7)$$

where

$$C_T = \frac{T}{\rho A_r v_T^2} \quad (8)$$

is the thrust coefficient of a rotor and

$$\sigma = \frac{N_b \bar{c}}{\pi r} \quad (9)$$

is the disc solidity ratio. Here  $v_T$  is blade tip speed,  $A_r = \pi r^2$  is the disc area of a rotor,  $N_b$  is the number of blades,  $\bar{c}$  is the rotor average chord and  $r$  is rotor radius.

In hover the thrust of a rotor is  $T = mg/N_R$ , and

$$\bar{c}_l = \frac{6T}{\rho A_r v_T^2 \sigma} = \frac{6mg}{N_R \rho r v_T^2 N_b \bar{c}} \quad (10)$$

Thus

$$v_T = \sqrt{\frac{6mg}{N_R \rho r N_b \bar{c} \bar{c}_l}} \quad (11)$$

Hence tip speed varies inversely with  $\sqrt{\bar{c}_l}$ . Choosing a low  $\bar{c}_l$  will result in higher tip speed, leading to high blade Reynolds number, which reduces the blade section lift coefficient. However, it will be seen later that the power required to overcome profile drag varies with  $v_T^3$ , hence increasing  $\bar{c}_l$  will ultimately result in lower profile power. However, advance ratio in forward flight must also be considered, and choosing  $\bar{c}_l = 0.4$  provides a good balance for preliminary design.

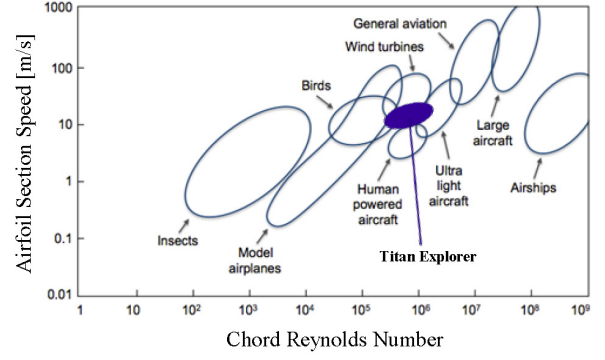


**Figure 4. Reynolds number and section speed for Titan rotary-wing aircraft.**

As an example, consider two distinct vehicle classes: a small 1 kg rotorcraft capable of acting as an ‘aerial scout’ from a fixed lander (designated ‘Bumblebee’) and a larger 350 kg rotorcraft (designated ‘TREx’ for Titan Rotary-wing Explorer). Nominal rotor parameters for both are given in the upper portion of Table 2.

For the 1kg vehicle (Bumblebee), the resulting rotor tip speed in hover (from Equation 11) is 21.6 m/s; rotor tip speed in hover for the 350 kg vehicle (TREx) is 35.5 m/s. With reference to Table 1, the tip Mach number can be computed from

$$Ma = \frac{v_T}{a} \quad (12)$$

Tip Mach number is 0.11 for Bumblebee and 0.18 for TREx. It is interesting to note that rotors operate in essentially incompressible flow ( $Ma < 0.3$ ), which may be counter-intuitive at first due to the lower speed of sound on Titan compared to Earth (Table 1); however, the reduced gravity and increased density outweigh the lower speed of sound.

For a hover-optimized rotor [14], blade chord  $c$  varies inversely with radial location and the rotational speed of a blade section varies as  $v = \frac{r}{R} v_T$ . Thus for an optimal blade the Reynolds number is constant along the blade and is equal to

$$Re = \frac{v_t c_T}{\nu} \quad (13)$$

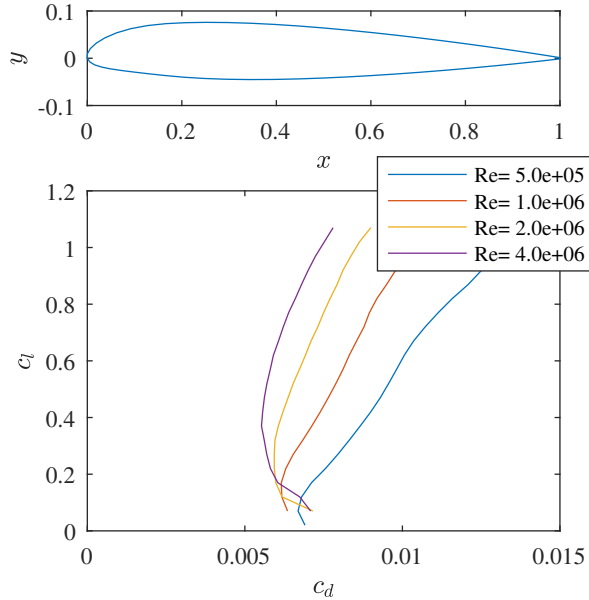
where  $\nu$  is kinematic viscosity and tip chord  $c_T = \frac{2}{3} \bar{c}$  for a hover-optimized rotor. Given Titan’s kinematic viscosity (Table 1),  $Re \approx 2.3 \times 10^5$  for Bumblebee and  $Re \approx 2.0 \times 10^6$  for TREx.

Figure 4 shows that the combination of blade sectional Reynolds numbers and average blade airspeed are at the intersection of human-powered aircraft, ultra-light aircraft, and wind turbines. This provides opportunities for Titan rotary-wing explorers being equipped with high-performance, i.e. low drag, airfoils that are also fairly insensitive to changes in surface roughness over the vehicle lifetime in remote operation.

A rotor under optimal hover conditions further assumes uniform inflow, constant blade section angle of attack  $\alpha$  and thus constant sectional lift coefficient  $c_l = \bar{c}_l$  along the blade span. For thin airfoils, section lift coefficient is  $c_l = c_{l_\alpha} (\alpha - \alpha_0)$ ,

**Table 2. Nominal rotor and vehicle parameters**

Parameter	Symbol	Bumblebee	TREx
number of rotors	$N_R$	2 (1 co-ax)	8 (4 co-ax)
blades per rotor	$N_b$	2	2
rotor radius	$R$	0.1 m	0.65 m
rotor mean chord	$\bar{c}$	0.02 m	0.10 m
blade mean lift coefficient (in hover)	$\bar{c}_l$	0.4	0.4
thrust coefficient	$C_T$	0.0170	0.0131
“empty” mass	$m_e$	0.75 kg	320 kg
body drag coefficient	$C_{D_{body}}$	0.5	0.5
frontal area	$S$	0.0121 m <sup>2</sup>	0.5 m <sup>2</sup>
drivetrain efficiency	$\eta$	0.81	0.81
battery energy density	$e_{batt}$	100 Wh/kg	100 Wh/kg
nominal battery mass	$m_{batt}$	0.25 kg	30 kg
nominal battery voltage	$V$	11.1	50 V
maximum battery current	$I_{max}$	10 A	100 A
hotel power during flight	$P_{hotel}$	20 W	100 W



**Figure 5. N.A.C.A. 23012 airfoil and drag polar**

where the lift-curve slope is  $c_{l_\alpha} = 2\pi$  and  $\alpha_0$  is the angle of attack that results in zero lift.

A candidate airfoil for a Titan rotorcraft is the N.A.C.A. 23012 (see Figure 5). Its zero-lift angle of attack is  $\alpha_0 = -1.2^\circ$ , and at  $c_l = 0.4$  the section drag coefficient varies from 0.006 to 0.009 (depending on Reynolds number). Given that both the Bumblebee and TREx have an assumed hover section lift coefficient of  $\bar{c}_l=0.4$ , the section angle of attack is  $\alpha = 2.4^\circ$  for both vehicles’ rotor blades. Note, however, that the blade twist will not be the same for both vehicles. At the tip, blade twist angle is

$$\theta_T = \alpha_T + \sqrt{\frac{C_T}{2}} [\text{rad}] \quad (14)$$

Hover thrust coefficients for both Bumblebee and TREx are given in Table 2, resulting in  $\theta_T = 7.7^\circ$  for Bumblebee and  $\theta_T = 7.1^\circ$  for TREx.

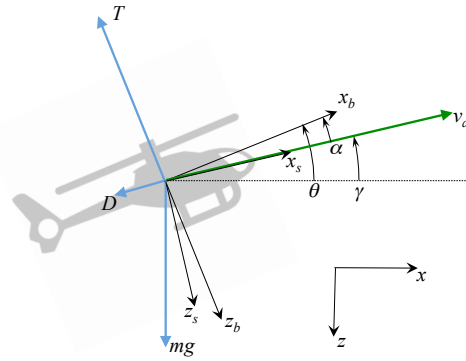


**Figure 6. Coordinate frames and forces in steady flight**

#### 4. ENERGETICS OF ROTARY-WING FLIGHT

The purpose here is to develop a model for the energy required for rotary-wing flight on Titan and to assess the sensitivity of required energy to basic vehicle parameters. Low-order models for drag and power will thus be used: once vehicle sizing has been determined, higher-order models can be used in performance analysis either to provide correction factors for the low-order models or used directly.

Referring to Figure 6 and considering a vehicle at constant speed flight,

$$T \sin \alpha = -D - mg \sin \gamma \quad (15)$$

$$T \cos \alpha = mg \cos \gamma \quad (16)$$

where  $T$  is total thrust,  $D$  is the body drag force,  $m$  is mass,  $g$  is acceleration due to gravity,  $\gamma$  is the flight path angle with respect to the local horizontal, and  $\alpha$  is the rotor disk’s angle of attack. The body drag force can be written as

$$D_{body} = qSC_{D_{body}} \quad (17)$$

where  $q = \frac{1}{2}\rho v_a^2$ ,  $S$  is a reference area and  $C_{D_{body}}$  is the body drag coefficient. This body drag term includes drag from all components that are not producing thrust.

In trimmed flight at a particular airspeed and flight path angle

one can solve for the required thrust and angle of attack:

$$\tan \alpha = \frac{-D_{body} - mg \sin \gamma}{mg \cos \gamma} \quad (18)$$

$$T = \sqrt{m^2 g^2 + D_{body}^2 + 2Dmg \sin \gamma} \quad (19)$$

and for rigid, fixed-pitch rotors, the body pitch angle is the sum of angle of attack and flight path angle:

$$\theta = \alpha + \gamma \quad (20)$$

The total aerodynamic power required to sustain constant speed flight comprises four parts: (1) parasite power (the dot product of the body drag force and the velocity vector); (2) induced power (caused by lift of the rotors); (3) profile power (caused by the drag of the rotor's airfoil); (4) power required to climb (the dot product of the velocity vector and the gravitational force):

$$P_{aero} = P_{parasite} + \kappa_{ind} P_{induced} + P_{profile} + P_{gravity} \quad (21)$$

Parasite power is

$$P_{parasite} = D_{body} v_a = q S C_{D_{body}} v_a \quad (22)$$

Induced power is

$$P_{induced} = T w \quad (23)$$

where  $w$  is the downwash in the rotor plane. Glauert's hypothesis relates thrust and downwash for a rotor with disc area  $A$  operating in a fluid with density  $\rho$ :

$$T = 2\rho A \bar{v} w \quad (24)$$

where  $\bar{v} = \sqrt{(w - v_a \sin \alpha)^2 + (v_a \cos \alpha)^2}$ . In hover  $v_a = 0$  and  $w$  can be computed directly; in forward flight it is computed iteratively.

Note the induced power factor  $\kappa_{induced}$  in Equation 21. The Glauert-derivation of induced power is a lower bound; McCormick suggests using  $\kappa_{ind} = 1.15$  [12].

Profile power is

$$P_{profile} = \rho A v_T^3 \frac{\sigma \bar{c}_{d,blade}}{8} (1 + 3\mu^2) \quad (25)$$

where  $v_T = \omega r$  is rotor tip speed,  $\bar{c}_{d,blade}$  is the average blade section drag coefficient,  $\sigma$  is rotor solidity ratio and  $\mu = \frac{v_a}{v_T}$  is advance ratio.

The average blade section drag coefficient depends on the choice of airfoil, the average blade Reynolds number, and the section lift coefficient. Averaged over one rotor revolution and accounting for the effect of forward flight, the average blade section lift coefficient is

$$\bar{c}_l = \frac{6C_T}{\sigma \left(1 + \frac{3\mu^2}{2}\right)} \quad (26)$$

Here it shall be assumed that thrust coefficient is constant (so that increasing thrust implies greater tip speed). Substituting

$\mu = \frac{v_a}{v_T}$  and using the definition of thrust coefficient (Equation 8), the average blade section lift coefficient is

$$\bar{c}_l = \frac{6C_T}{\sigma \left(1 + \frac{3v_a^2 \rho A C_T}{2T}\right)} \quad (27)$$

Given  $\bar{c}_l$  and Reynolds number, average section drag coefficient can be determined from airfoil data.

Gravity power is

$$P_{gravity} = mg v_a \sin \gamma \quad (28)$$

For negative flight path angle (i.e. descending flight), gravity power will be negative; for constant altitude flight,  $\gamma = 0$  and  $P_{gravity} = 0$ .

The net power drawn from the battery during flight is the aerodynamic power (conditioned by the net drivetrain efficiency, i.e. the efficiency of converting power extracted from the battery to the shaft) and hotel power (the power required to run vehicle avionics, scientific instruments, and thermal management):

$$P_{net} = \frac{P_{aero}}{\eta} + P_{hotel} \quad (29)$$

Endurance is

$$t_e = \frac{m_{batt} e_{batt}}{P_{net}} \quad (30)$$

where  $e_{batt}$  is battery energy density and  $m_{batt}$  is battery mass. Since total power varies with airspeed, endurance varies with airspeed.

Range is

$$R = t_e v_g = \frac{m_{batt} e_{batt}}{P_{net}} v_g \quad (31)$$

where  $v_g$  is the ground speed. For simplicity it shall be assumed that winds are calm (so that  $v_g = v_a$ ). Range also varies with airspeed. As with a fixed-wing aircraft, the flight condition that maximizes endurance is not the condition that maximizes range: maximum endurance occurs when total power is minimized; maximum range occurs when  $\frac{P_{net}}{v_g}$  is minimized.

## 5. PERFORMANCE AND SENSITIVITY

Remaining vehicle parameters that are required for performance analysis are summarized in the lower portion of Table 2 both the 1 kg vehicle and the 350 kg vehicle. Note the relatively low battery energy density (well over 150 Wh/kg is currently available in commercial hobby-grade lithium-polymer batteries): mass of components associated with battery temperature control is included in the battery pack mass, reducing the net energy density of the pack.

*TREx*

Figure 7 shows the contributions to total required aerodynamic power at Titan sea level as a function of airspeed. Total

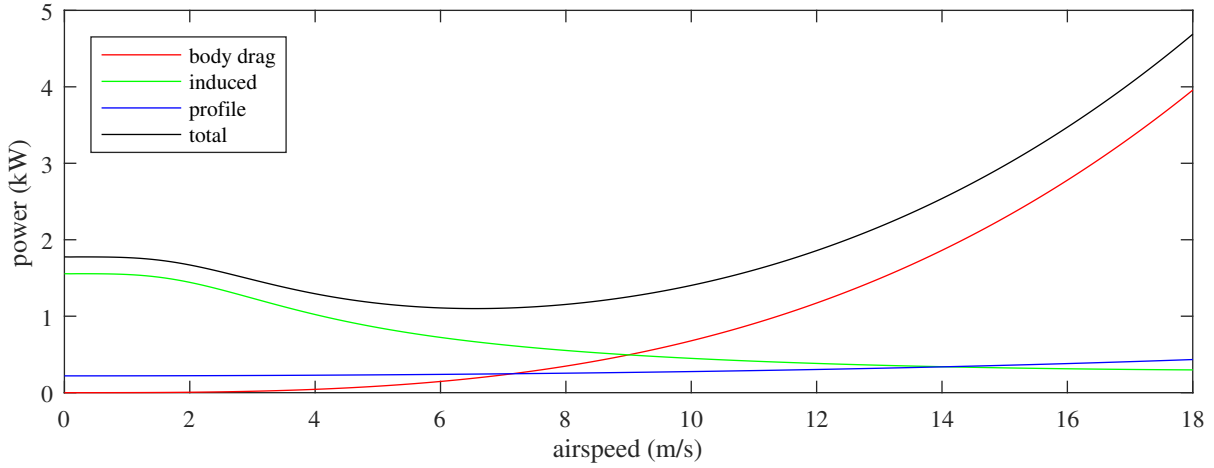


**Figure 7. TREx contributions to aerodynamic power required for level flight at Titan surface.**

hover power is 1.87 kW, with the largest contribution coming from induced power.

Comparing total hover power with the ideal hover power, the vehicle's figure of merit is

$$FM = \frac{P_i}{P_{hover}} = \frac{1}{P_{hover}} \sqrt{\frac{m^3 g^3}{2\rho A}} = 0.72 \quad (32)$$

There is a clear minimum in total power at an airspeed of 6.5 m/s (23.4 km/h): this is the flight condition that maximizes endurance (see Figure 8, upper plot). The maximum range flight condition occurs when  $\frac{P}{v}$  is minimized (i.e. the point at which a line starting at  $P = 0, v = 0$  is tangent to the total power curve). This occurs at 9.5 m/s (see Figure 8, lower plot). Given the vehicle parameters of Table 2, the maximum endurance is 2.06 hours and the maximum range is nearly 60 km.

Vehicle body drag becomes the largest contributor to required aerodynamic power when airspeed exceeds 9 m/s. Reducing body drag coefficient or the frontal area of the body will thus improve range, but will not have a significant effect on endurance.

Vehicle trim condition (body pitch, net thrust, and advance ratio) are shown in Figure 9. In a rigid-rotor multi-copter, body pitch angle is equal to rotor pitch angle, and nose-down (i.e. negative) pitch is required for forward flight. Since the vertical component of total thrust must equal the weight of the vehicle (and because the horizontal component of total thrust acts to overcome drag), total thrust increases as airspeed increases.

Advance ratio has a significant effect on performance. For traditional (i.e. articulated rotor) helicopters with flexible blades, advance ratios above approximately 0.3 are likely to lead to significant blade flapping and challenges in roll trim. In the case of coaxial helicopters with rigid blades, significantly higher advance ratios can be flown (up to 0.4). For the TREx configuration, advance ratio exceeds 0.3 at 10.7 m/s, and exceed 0.4 at 14.5 m/s. This is well above the maximum range airspeed of 9.5 m/s.

Motor conditions (rpm, torque, power) are shown in Figure 10. It is assumed that for an X-8 multi-copter (four co-

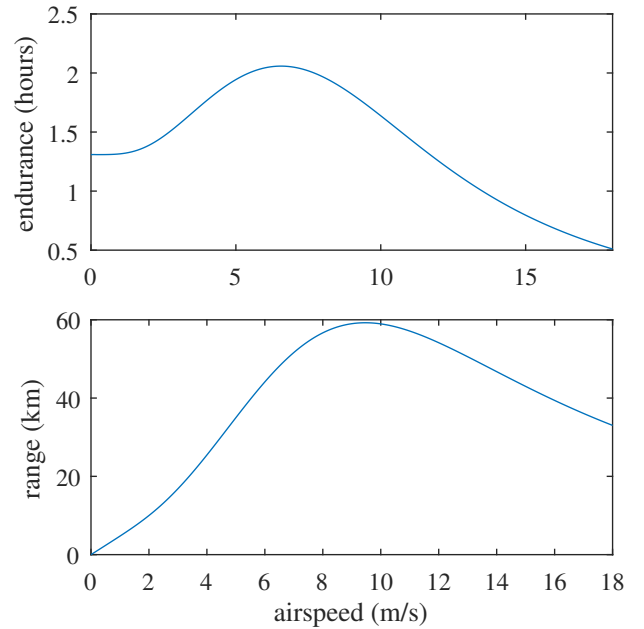


**Figure 8. TREx endurance and range**

axial rotors arranged in an “X” configuration), the total power is divided equally among the eight motors, and the torque required from a motor is computed from

$$P_{motor} = \tau\omega \quad (33)$$

Brushless motors that can provide over 800W continuous power are readily available in hobby motors (indeed, motors with well over 5 kW continuous power can be easily sourced). However, these high-power commercially available motors generally have motor constants ranging from 100 rpm/V to 200 rpm/V, which is too high for TREx. Assuming the motors are operating at 50V, achieving 550 rpm with an un-g geared drive system implies that the motor constant should be close to 15 rpm/V (and of course hobby-grade motors would not be suitable for a space mission).

Total power contours in Figure 11 can be used to determine maximum speed as well as the absolute ceiling given total power available.

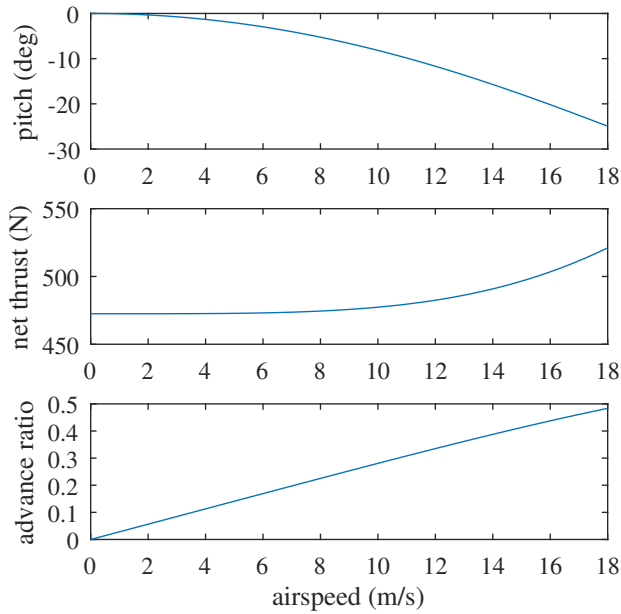


**Figure 9. TREx rotor and body trim**

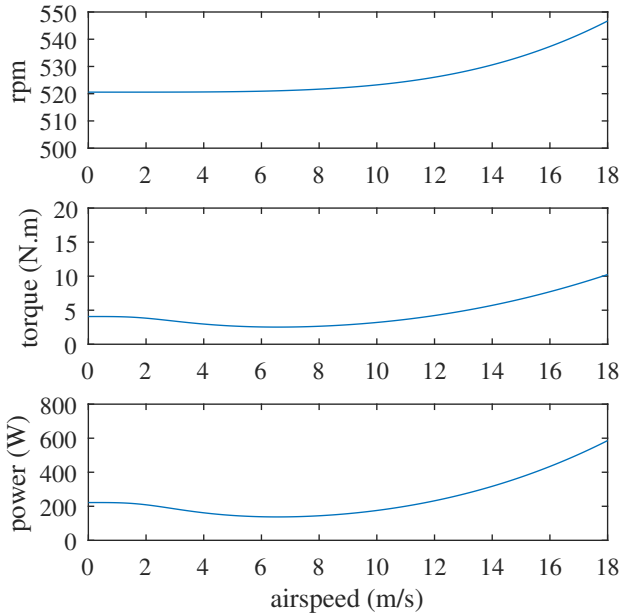


**Figure 10. TREx motor requirements**

Assuming: the motor power system operates at 50 V; a maximum of 100A can be drawn from the propulsion battery; and net drivetrain efficiency of 81% (90% motor efficiency and 90% efficiency in the electronic speed controller), the net power available to the shaft is 4050W. The maximum level flight speed at the surface is thus approximately 17 m/s (61 km/h); the hover ceiling is 32 km; and the absolute ceiling is 45 km. There is a possibility of methane “freezing rain” above 12 km altitude [15], hence the operational ceiling is likely to be determined by weather conditions on Titan and not by vehicle capability.

#### Bumblebee

Total electrical power of a small Titan flight vehicle is roughly 30 W [3]. Only a small fraction of this total is required

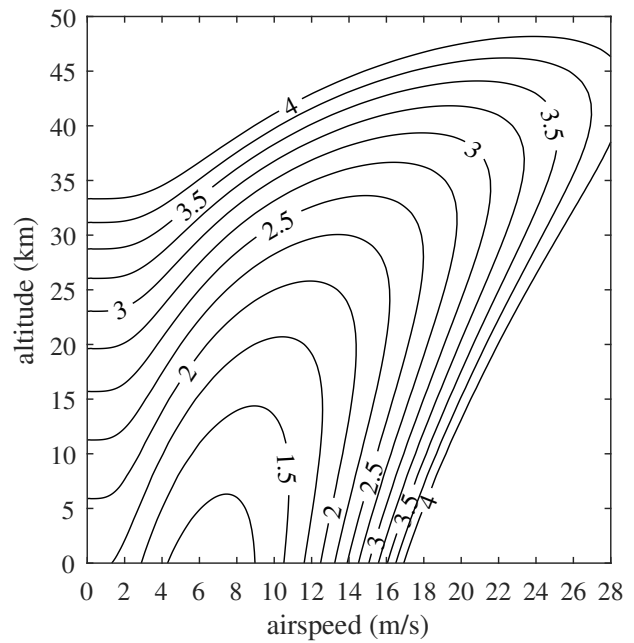


**Figure 11. Total shaft power required (in kilowatts) for level flight as function of airspeed and altitude for TREx.**

for flight: ideal hover power for a 1 kg vehicle with 0.2 m rotor diameter operating on Titan is 2.7 W; even with a fairly conservative figure of merit of 0.6 the hover power is less than 4.5 W. For comparison, the power required to run vehicle systems (autopilot, telemetry, heaters) is approximately 20 W (5 W for autopilot and flight computer, 5 W for telemetry, 10 W for heating). This hotel power is thus the largest contributor to energy required for flight, and should be explicitly accounted for in any analysis of vehicle performance. Indeed, the fact that such a large fraction of mission energy for a small vehicle must be spent on heating in the cold Titan atmosphere motivated the appellation ‘Titan Bumblebee’ - bumblebees are subarctic insects whose thermal management is critically optimized - they do not drain flowers completely because doing so would allow their flight muscles too cool, requiring energy to warm up again. Instead they fly away earlier, maximizing overall efficiency.

Figure 12 shows the contributions to total required aerodynamic power at Titan sea level as a function of airspeed. Total hover power is 3.63 W, with the largest contribution coming from induced power. Ideal hover power is 2.69 W.

Comparing total hover power with the ideal hover power, the vehicle’s figure of merit is

$$FM = \frac{P_i}{P_{hover}} = \frac{1}{P_{hover}} \sqrt{\frac{m^3 g^3}{2\rho A}} = 0.74 \quad (34)$$

There is a clear minimum in total aerodynamic power at an airspeed of 3 m/s (10.8 km/h): this is the flight condition that maximizes endurance (see Figure 13, upper plot).

Note that hotel power is assumed to be 20W (Table 2): this is significantly greater than the aerodynamic power required for flight, and thus has a significant impact on endurance, range, and the speed at which maximum range is achieved.

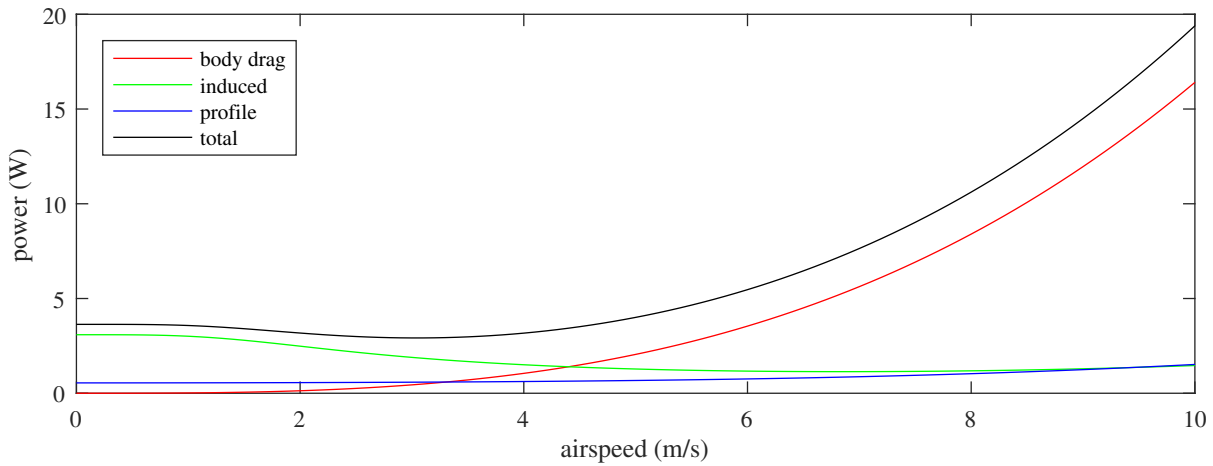


**Figure 12. Bumblebee contributions to aerodynamic power required for level flight at Titan surface.**

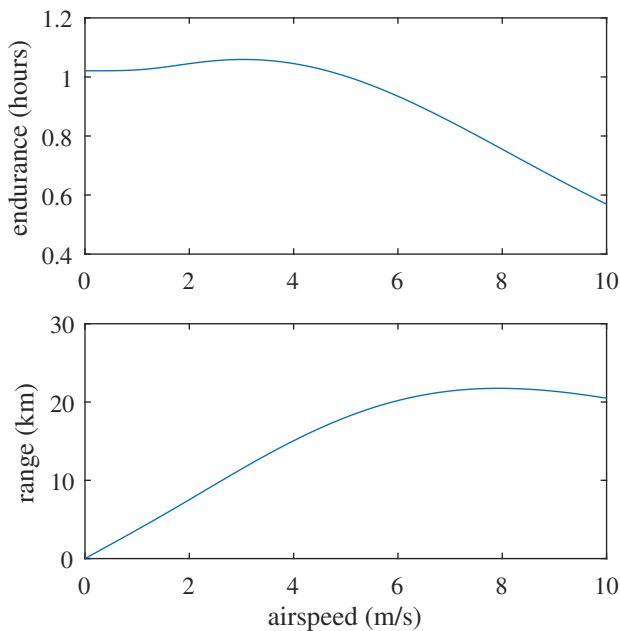


**Figure 13. Bumblebee endurance and range**

Minimum aerodynamic power is 2.92 W and occurs at 3 m/s (Figure 12). Minimum net power drawn from the battery (which includes drivetrain efficiency and hotel power) is 23.6 W; a battery with mass 0.25 kg will thus provide 1.06 hours endurance. Vehicle body drag becomes the largest contributor to required power when airspeed exceeds 9 m/s. Reducing body drag coefficient or the frontal area of the body will thus improve range, but will not have a significant effect on endurance. Maximum range is 22 km, and the airspeed that maximizes range is 8 m/s (17.6 km/h).

Rotor and body trim are plotted in Figure 14. Significant pitch is required to achieve the maximum range flight speed: recall that range is significantly affected by hotel power, hence the speed for maximum range is high (intuitively, higher speed results in less hotel energy expended for a given distance flown). High speed necessitates greater body pitch angle. Advance ratio remains below 0.4 well above the maximum range speed.

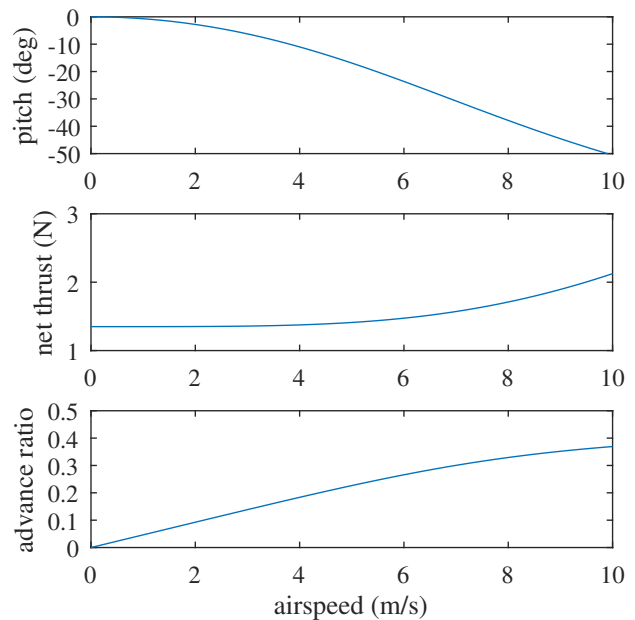


**Figure 14. Bumblebee rotor and body trim**

Motor condition is plotted in Figure 15. Motor speed, torque, and power are well within the capabilities of brushless electric motors, but challenges related to cryogenic operation will have to be addressed.

Power contours for level flight are plotted in Figure 16. Assuming that 8 W are available to the shaft (this represents 0.8 A at 10 V), Bumblebee's absolute ceiling is nearly 40 km.

## 6. CONCLUSION

This paper has discussed the power requirements of rotary-wing flight on Titan, focusing on a "repositionable lander" and on a small "aerial scout" vehicle. The envisioned flight operation consists of periods of battery-powered flight followed by recharge using a Multi-Mission Radioisotope Thermoelectric Generator.

In both cases the aircraft are capable of performing scientific

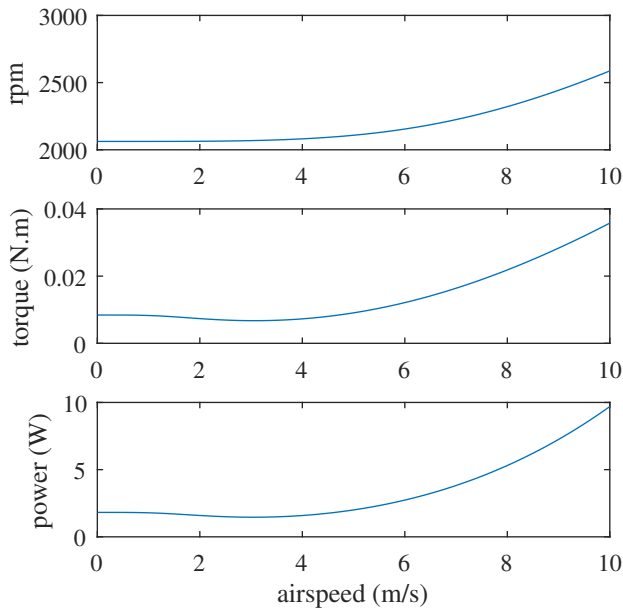


**Figure 15. Bumblebee motor requirements**

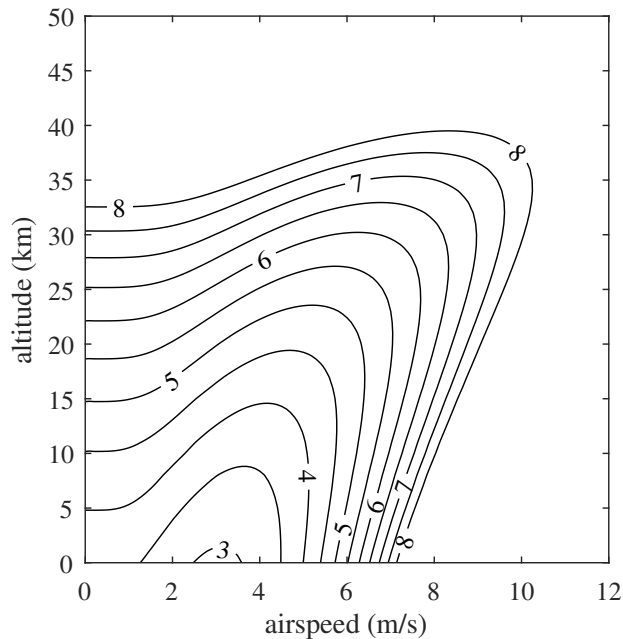


**Figure 16. Total shaft power required (in watts) for level flight as function of airspeed and altitude for Bumblebee.**

ically useful missions, with the 350kg-class vehicle capable of 2 hours maximum endurance and 60 km maximum range and the 1kg-class vehicle capable of 1 hour endurance and 20 km maximum range. The operational ceiling is likely to be limited by weather: both vehicles can maintain steady level flight at altitudes exceeding 40 km, but the likelihood of methane icing on the airframe above 12 km altitude may limit flight operations.

The greatest contributor to aerodynamic power at higher speeds is body drag: reducing either the body drag coefficient and/or the body frontal area has the greatest potential to improve flight performance.

## REFERENCES

- [1] R. D. Lorenz, "Post-cassini exploration of titan: science rationale and mission concepts," *Journal of the British Interplanetary Society*, vol. 53, pp. 218–234, 2000.
- [2] L. A. Young, "Exploration of titan using vertical lift aerial vehicles," in *Forum on Innovative Approaches to Outer Planetary Exploration 2001-2020*, January 2001.
- [3] R. D. Lorenz, "Titan bumblebee: a 1kg lander-launched UAV concept," *Journal of the British Interplanetary Society*, vol. 61, pp. 118–124, 2008.
- [4] G. E. Dorrington, "Concept options for the aerial survey of titan," *Advances in Space Research*, vol. 47, pp. 1–19, 2011.
- [5] J. W. Barnes, L. Lemke, R. Foch, C. P. McKay, R. A. Beyer, J. Radebaugh, D. H. Atkinson, R. D. Lorenz, S. L. Mouelic, S. Rodriguez, J. Gundlach, F. Gianini, S. Bain, F. M. Flasar, T. Hurford, C. M. Anderson, J. Merrison, M. Adamkovics, S. A. Kattenhorn, J. Mitchell, D. M. Burr, A. Colaprete, E. Schaller, A. J. Friedson, K. S. Edgett, A. Coradini, A. Adriani, K. M. Sayanagi, M. J. Malaska, D. Morabito, and K. Reh, "AVIATR- Aerial Vehicle for In-situ and Airborne Titan Reconnaissance," *Exp Astronomy*, vol. 33, pp. 55–127, 2012.
- [6] K. Reh, T. Magner, D. Matson, A. Coustenis, J. Lunine, J.-P. Lebreton, C. Jones, and J. Sommerer, "Titan saturn system mission study 2008: Final report," NASA, Task Order NM0710851, January 2009.
- [7] R. D. Lorenz, "A review of balloon concepts for Titan," *Journal of the British Interplanetary Society*, vol. 61, pp. 2–13, 2008.
- [8] J. S. Levine and H. S. Wright, "Titan explorer: the next step in the exploration of a mysterious world," NASA, Tech. Rep., June 2005.
- [9] J. L. Hall, V. V. Kerzhanivich, A. H. Yavrouian, J. A. Jones, C. V. White, B. A. Dudik, G. A. Plett, J. Mennella, and A. Elfes, "An aerobot for global in situ exploration of titan," *Advances in Space Research*, December 2006.
- [10] P. Backes, W. Zimmerman, J. Jones, and C. Gritters, "Harpoon-based sampling for planetary applications," in *IEEE Aerospace Conference*. Big Sky, Montana: Institute for Electrical and Electronics Engineers, March 2008.
- [11] R. Prakash, R. D. Braun, L. S. Colby, S. R. Francis, M. E. Gunduz, K. W. Flaherty, J. M. Lafleur, and H. S. Wright, "Design of a long endurance titan vtol vehicle," in *IEEE Aerospace Conference*. Big Sky, Montana: Institute for Electrical and Electronics Engineers, March 2005.
- [12] B. W. McCormick, *Aerodynamics, Aeronautics, and Flight Mechanics*, 2nd ed. Hoboken, NJ: John Wiley and Sons, Inc., 1995.
- [13] R. D. Lorenz, "Titan here we come," *New Scientist*, pp. 24–27, July 15 2000.
- [14] A. Gessow and G. C. Myers, *Aerodynamics of the Helicopter*. New York: Frederick Ungar Publishing, 1985.
- [15] R. D. Lorenz and J. I. Lunine, "Titan's snowline," *Icarus*, vol. 158, pp. 557–559, 2002.

## BIOGRAPHY



**Jack W. Langelaan** is an Associate Professor in the Department of Aerospace Engineering at Penn State University. His research focuses on path planning, control, state estimation and data fusion, applied especially to navigation, obstacle avoidance, and long-range flight of small uninhabited aircraft. In 2011 he was leader of Team Pipistrel-USA.com, winner of the NASA/CAFE Green Flight

Challenge with the Taurus G4 aircraft. He has taught undergraduate classes in dynamics and control, aircraft flight dynamics, introductory aeronautics, and capstone aircraft design; he has taught graduate courses in state estimation and global navigation satellite systems. He received his Ph.D. in Aeronautics and Astronautics from Stanford University in 2006, a Master of Science in Aeronautics and Astronautics from the University of Washington in 1994, and a Bachelor of Applied Science in Engineering Physics from Queens University in 1992. From 1995 to 2000 he worked as an engineer at Bombardier Aerospace in Toronto, Canada. Langelaan is an Associate Fellow of the American Institute of Aeronautics and Astronautics, serving on the Guidance, Navigation and Control Technical Committee and on the Transformational Flight Program Committee.



**Sven Schmitz** is an Associate Professor in the Department of Aerospace Engineering at Penn State University. He received a diploma degree in Aerospace Engineering from RWTH Aachen (Germany) in 2002 and a Ph.D. in Mechanical and Aeronautical Engineering from the University of California Davis in 2006. Sven spent four years as a post-doctoral researcher and project scientist

at Davis before coming to Penn State. He is an expert in rotary wing aerodynamics with an emphasis on vortical flows. His growing research program embraces the areas of wind turbine aerodynamics and rotorcraft aeromechanics. Current activities include wind farm wake modeling, icing on wind turbines, rotor hub flows, and rotor active control.



**Jose Palacios** obtained his Ph.D. in May 2008. His doctorate thesis focused on ultrasonic de-icing for helicopter rotor blades. Dr. Palacios continued his post-doctoral studies at Penn State investigating ultrasonic de-icing for helicopter rotors. To aid his research in the field of rotor blade ice accretion and protection, he designed and constructed a novel Adverse Environment Rotor Test Stand

in which icing cloud conditions representative of rotorcraft icing can be reproduced. In 2011, Jose became a Research Associate with the Aerospace Engineering Department at the Pennsylvania State University where he continues investigations in the fields of rotorcraft de-icing, rotor blade and engine icing physics, and rotor blade control surfaces for performance enhancements and vibration control. In 2013, Jose became a tenure-track professor at The Pennsylvania State University, where he works areas of research that include structural dynamics, rotor blade, engine, and wind turbine icing, and rotorcraft aeromechanics. In 2015, he designed and constructed an icing wind tunnel at the Pennsylvania

State University for the testing of partially melted crystals responsible for engine icing and also for testing of airframe icing to UAV configurations.



**Ralph Lorenz** has a B.Eng. in Aerospace Systems Engineering from the University of Southampton in the UK and a Ph.D. in Physics in 1994 from the University of Kent at Canterbury. He worked 1990-1991 for the European Space Agency on the design of the Huygens probe and during his PhD research designed and built its penetrometer instrument that 12 years later measured

the mechanical properties of Titans surface when Huygens landed in January 2005. From 1994-2006 he worked as a planetary scientist at the Lunar and Planetary Laboratory, University of Arizona with particular interests in Titan, Mars, planetary climate, nonequilibrium thermodynamics, aerospace vehicles and radar. He continues to work on those topics as Senior Professional Staff at the Johns Hopkins University Applied Physics Laboratory in Laurel, MD. He is on the editorial board of the International Journal of Astrobiology and is author or co-author of several books including *Lifting Titans Veil*, *Spinning Flight*, and *Space Systems Failures* as well as over 150 publications in refereed journals.